







Article

Numerical Analysis of the Influence of Empty Channels Design on Performance of Resin Flow in a Porous Plate

Glauciléia M. C. Magalhães ¹, Cristiano Fragassa ^{2,*} , Rafael de L. Lemos ³ ,
Liércio A. Isoldi ^{1,3} , Sandro C. Amico ⁴ , Luiz A. O. Rocha ⁵, Jeferson A. Souza ^{1,3} 
and Elizaldo D. dos Santos ^{1,3} 

¹ Graduate Program of Computational Modeling, Federal University of Rio Grande, Italia Avenue, km 8, Rio Grande 96201-900, Brazil; mglaucileia@gmail.com (G.M.C.M.); liercioisoldi@furg.br (L.A.I.); jefersonsouza@furg.br (J.A.S.); elizaldosantos@furg.br (E.D.d.S.)

² Interdepartmental Center for Industrial Research on Advanced Applications in Mechanical Engineering and Materials Technology, University of Bologna, Viale Risorgimento 2, 40136 Bologna, Italy

³ Graduate Program of Ocean Engineering, Federal University of Rio Grande, Avenue, km 8, Rio Grande 96201-900, Brazil; er.lemos@outlook.com

⁴ Materials Engineering Graduate Program, University of Rio Grande do Sul, Bento Gonçalves Av., 9500, Porto Alegre 91501-970, Brazil; amico@ufrgs.br

⁵ Mechanical Engineering Graduate Program, University of Vale do Rio dos Sinos, São Leopoldo 93022-750, Brazil; luizor@unisinis.br

* Correspondence: cristiano.fragassa@unibo.it; Tel.: +39-347-697-4046

Received: 19 March 2020; Accepted: 17 April 2020; Published: 11 June 2020



Featured Application: The influence of empty channel design on resin flow in a porous plate is studied. Constructal design is used for geometric investigation of I and T-shaped channels. The multiphase resin/air flow in the porous plate is solved numerically. T-shaped configurations with long branches lead to the best impregnation performance. Permanent air voids arise in the domain for very thin T-shaped channels.

Abstract: This numerical study aims to investigate the influence of I and T-shaped empty channels' geometry on the filling time of resin in a rectangular porous enclosed mold, mimicking the main operating principle of a liquid resin infusion (LRI) process. Geometrical optimization was conducted with the constructal design (CD) and exhaustive search (ES) methods. The problem was subjected to two constraints (areas of porous mold and empty channels). In addition, the I and T-shaped channels were subjected to one and three degrees of freedom (DOF), respectively. Conservation equations of mass and momentum for modeling of resin/air mixture flow were numerically solved with the finite volume method (FVM). Interaction between the phases was considered with the volume of fluid method (VOF), and the effect of porous medium resistance in the resin flow was calculated with Darcy's law. For the studied conditions, the best T-shaped configuration resulted in a filling time nearly three times lower than that for optimal I-shaped geometry, showing that the complexity of the channels benefited the performance. Moreover, the best T-shaped configurations were achieved for long single and bifurcated branches, except for configurations with skinny channels, which saw the generation of permanent voids.

Keywords: constructal design; resin flow; porous media; numerical simulation; filling time

1. Introduction

Liquid composite molding (LCM) processes were developed to enable the production of large, wide, and complex structural components at low cost. Among the important LCM processes, it is important to mention liquid resin infusion (LRI), which consists of the injection of a polymer resin through empty channels mounted on a fibrous mold, favoring the global propagation of the resin over the mold domain [1]. One of the most considerable difficulties in applying LRI is related to complete mold filling and void formation, ensuring that the fibrous reinforcement is completely impregnated by the resin within the mold [2–5].

To tackle the reported difficulties, several efforts have been made to improve process comprehension, as well as to avoid traditional trial-and-error approaches. One possibility is the use of computational tools to simulate multiphase resin/air flow into the enclosed mold [3–8]. The study of parametrical investigations in the LRI process (as the influence of design over the behavior of resin/air flow, voids formation, and filling time) also represents an important subject. Therefore, studies have been carried out in the analytical, experimental, and numerical scope to improve the understanding of resin/air flow in this kind of domain [3,4].

The development of computational methods for the representation of LCM processes is an important point of concern. For example, Isoldi et al. [9] performed a numerical study of resin flow in porous domains that mimics the operational principle of the Resin Transfer Molding (RTM) and Light Resin Transfer Molding (LRTM) processes. Different resin flow cases were solved numerically (linear, radial, and complex three-dimensional domain) and compared with analytical, experimental, and numerical results available in the literature. The maximum difference between these solutions was about 8.0%, showing the validity of the developed numerical method. Wang et al. [1] conducted a numerical and experimental study of the resin infusion process under industrial conditions. The authors verified that mold filling time determined by numerical simulation brought about results in agreement with experimental solutions. Afterward, Grössing et al. [10] compared the technical feasibility of using two different numerical methods (PAM-RTM[®] and OpenFOAM) to obtain numerical solutions of resin flow. Firstly, it was found that the numerical methods led to valid solutions in comparison with experimental results. It was also verified that both numerical methods had very similar results for the simulation of resin flow in porous media. Sirtautas et al. [11] developed a numerical model based on the Finite Element Method (FEM), considering the effects of compressibility and orthotropic permeability dependent on pressure in the domain for different fibrous materials. A comparison between the numerical model and experimental results was performed for resin flow in the two-dimensional domain of an aerospace piece. The results showed good agreement, recommending the use of the proposed computational method. Pierce et al. [12] developed and validated a multi-physics model to improve the simulation of the infusion process in the complex preform. The results are compared with traditional models that do not consider fabric deformation. The combination of deformation-dependent permeability properties and the preform draping model led to more realistic predictions for local infusion flow. Chebil et al. [13] developed a computational model for the simulation of three-dimensional resin flow in laminated preform composed of multiple layers with different permeabilities. The method proposed the use of shell elements for flow simulation instead of solid elements, leading to a reduction in computing time. Rubino and Carlone [14] proposed an analytical/numerical methodology to consider the effects of preform compaction on resin flow for a deformable porous media, which is important for processes such as vacuum assisted resin transfer molding (VARTM) and Seeman composites resin infusion molding process (SCRIMP), where a flexible bag is generally used as part of the mold. The results showed that preform compaction affected resin flow and filling time.

The numerical approach has also been used to define strategies for several LCM processes. Examples of the evaluation of gate placements in RTM processes seeking to prevent void content and minimize filling time had been widely reported in different works [15–20]. The work of Brouwer et al. [3] proposed strategies to improve the positioning of injection channels in one LRI process using

computational modeling. More precisely, the authors presented developments in two large structures to be filled with resin, a rotor blade, and a boat hull 20 m and 16 m long, respectively. The strategy adopted by the authors consisted of a main injection channel in the central region of the domain (the keel for the case of injection in the hull domain) with several bifurcated channels spread along the area of the domain (from the center to the periphery). Afterward, Gomes et al. [21] performed a numerical and experimental study for better characterization of a VARTM (vacuum assisted resin transfer molding) process, indicating the best strategies for the filling of a C-shaped stringer. The results indicated that the consideration of two exit regions (with vacuum) and one entering region of resin placed in the extremes of domain length was the best strategy to minimize filling time and prevent void formation. Wang et al. [1] developed an iterative method based on a centroidal Voronoi diagram for optimization of the distribution of several channels to reduce the number of required tests.

Recently, Struzziero and Skordos [22] performed a numerical multi-objective optimization focusing on the choice of an optimal temperature profile, which minimizes the filling time and the risk of hindering resin flow due to excessive curing. For the optimization, the authors employed the genetic algorithm (GA) method. It achieved reductions of nearly 66% and 15% in filling time and final degree of cure, respectively, in comparison with standard solutions. Geng et al. [23] investigated the behavior of resin impregnation in curved porous plates mimicking a VARTM process. They performed an experimental study investigating the influence of curvature angles and preform layers on the advancement of the resin front line. The results indicated that due to interaction between the preforms and void formation, the curved regions led to an augmentation of 15% to 30% of filling time in comparison with a linear region. Shevtsov et al. [24] performed an experimental and numerical study for the manufacturing of three-dimensional composite parts of complex shape. For the computational model, a numerical technique based on liquid resin flow into porous preform is coupled with a model that describes the fluid motion in unsaturated soils. The developed method allowed the prediction of inner and outer dry spots depending on the resin flow movement. Despite several important works reported, few studies can be found on the evaluation of the influence of the geometry of empty channels in the behavior of resin/air fluid flow into the porous domain. In the present study, a geometrical optimization of I and T-shaped empty channels over the required time to fill a porous rectangular plate is performed with the constructal design (CD) and exhaustive search (ES) methods.

Constructal design is a method for assessment of design in any finite flow system based on the objectives and constraints principle. This method has been widely applied to show that shape and structure in nature (trees, rivers, animal body, and others) are deterministically generated following a physical principle named Constructal Law of Design and Evolution [25–29]. According to Bejan [28], constructal law states that the design of the finite-size flow system to persist in time (to live) must evolve freely to maximize access to its internal currents. This method has also been applied as a powerful tool to improve the design of several engineering problems as cooling systems, heat exchangers, renewable energy, transport systems, and even solid mechanics [30–36]. As per the authors' knowledge, except for the works of Refs. [37,38], the constructal design method has not been employed in the literature for investigation on the influence of geometry over impregnation of resin in a porous medium, which mimics the LRI process, a novelty in the present work.

Here, the application of computational modeling, constructal design, and exhaustive search (ES) in geometrical optimization of I and T-shaped empty channels inserted into the rectangular porous medium is proposed. The main aims here are to minimize the filling time of resin impregnation in the porous medium, prevent the formation of permanent voids in the domain, and investigate the influence of geometry over the performance indicator of the system. The solution domain is presented in a two-dimensional rectangular plate with a porous medium, which simulates a fibrous reinforcement. This work is a sort of continuity of the study by Magalhães et al. [38] with the difference being that here the T-shaped channel is completely optimized, i.e., all three degrees of freedom are investigated. The conservation equations of mass, momentum, and one equation for the transport of volumetric fractions are solved with the finite volume method (FVM) [39–41]. To deal with the resin/air interface

flow, the volume of fluid (VOF) method is used [42]. In the region of the porous medium, it is also considered a body force modeled with Darcy's law. More precisely, the simulations were performed using the computational fluid dynamics code FLUENT [41].

2. Mathematical Modeling

In this study, incompressible, laminar, and transient flow of a resin/air mixture in a two-dimensional domain is considered. Moreover, the two phases are treated as immiscible. For the prediction of this kind of flow, conservation equations of mass and momentum for the mixture of resin/air and one transport equation for prediction of resin volume fraction are numerically solved. The conservation equations of mass and momentum for the resin/air mixture are given by [43]:

$$\frac{\partial \rho}{\partial t} + \nabla \cdot (\rho \vec{V}) = 0 \quad (1)$$

$$\frac{\partial (\rho \vec{V})}{\partial t} + \nabla \cdot (\rho \vec{V} \vec{V}) = -\nabla P + \nabla \cdot \bar{\bar{\tau}} + \vec{F} \quad (2)$$

where ρ is the mixture density (kg/m^3), \vec{V} is the velocity vector (m/s), t is the time (s), μ is the dynamic viscosity of the fluid (Pa.s), ∇P is the pressure gradient (Pa/m), \vec{F} is an external force vector per unit volume (N/m^3) and $\bar{\bar{\tau}}$ is the stress tensor of the fluid (N/m^2), given by:

$$\bar{\bar{\tau}} = \mu \left(\nabla \vec{V} + \nabla \vec{V}^T \right) \quad (3)$$

The effect of the porous medium is included in the mathematical model by the insertion of a body force in the momentum equation based on Darcy's law, as given by [43–45]:

$$\vec{F} = -\frac{\mu}{K} \vec{V} \quad (4)$$

To tackle the resin/air mixture, the volume of fluid (VOF) method is employed [42]. In this approach, an additional transport equation for resin volume fraction (f) is necessary to define the quantity of resin along with each cell of the domain. This transport equation is given by [42]:

$$\frac{\partial f}{\partial t} + \nabla \cdot (f \vec{V}) = 0 \quad (5)$$

With the definition of volume fraction, density and dynamic viscosity in each cell of the computational domain can be calculated by [46]:

$$\rho = f \rho_{res} + (1 - f) \rho_{air} \quad (6)$$

$$\mu = f \mu_{res} + (1 - f) \mu_{air} \quad (7)$$

2.1. Problem Description

As previously mentioned, an incompressible, laminar, and transient multiphase flow of resin/air was considered, moving through a two-dimensional plate domain composed of a porous medium, as shown in Figure 1a,b. Empty channels are inserted along the porous domain to facilitate impregnation of the resin throughout the mold. In Figure 1a,b, these channels (I and T-shaped, respectively) are represented by the dark gray region, while the porous region is represented by light gray.

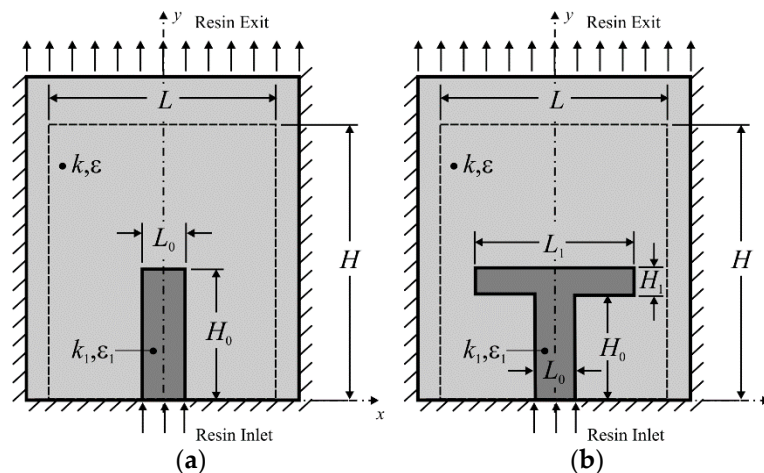


Figure 1. Computational domain of the problem, which mimics the liquid resin infusion (LRI) process with two empty channel geometries: (a) I-shaped, (b) T-shaped.

In both cases, flow is imposed by a pressure difference between the resin inlet (lower surface of the empty channel) and the exit region of multiphase flow (upper surface of the porous medium). Inlet pressure of $P_{in} = 1 \times 10^5$ Pa is considered, and pressure of $P_{out} = 0$ Pa is imposed in the exit. It is worth mentioning that, in a real LRI process, resin flow is driven by vacuum imposition at the exit of the fibrous reinforcement. Despite this, a pressure difference with the imposition of positive pressure in the resin inlet surface is represented. For computational modeling, it is important to predict the pressure difference. Hence, the imposition made here led to the same results as that achieved when the same pressure difference is imposed with the vacuum in the domain exit. In the remaining domain, bottom, and lateral surfaces, a non-slip and impermeability boundary condition is imposed ($u = v = 0$ m/s). For the resin volume fraction (Equation (5)), $f = 1$ at the inlet section and zero gradients (normal to the surface) on all the other surfaces are imposed. Concerning the physical properties of the resin and air, densities of $\rho_{res} = 916$ kg/m³ and $\rho_{air} = 1.225$ kg/m³ and dynamic viscosities of $\mu_{res} = 0.06$ kg/(ms) and $\mu_{air} = 1.7894 \times 10^{-5}$ kg/(ms) are adopted. For the porous media, a permeability of $K = 3.0 \times 10^{-10}$ m² and porosity of $\varepsilon = 0.88$ is imposed.

2.2. Geometrical Evaluation

Geometrical optimization was done by using an association between constructal design and exhaustive search, as explained in recent literature [47]. Figure 2 illustrates the main steps employed for optimization of the problem. Steps 1 to 3 presents the flow system and identifies a performance indicator (here, it is filling time). Steps 4 and 5 show the constraints of the problem, degrees of freedom, and the main parameters of the physical problem. It is also necessary to understand the physical problem and define a method for its solution (numerical solution in this case).

With the defining of geometry and understanding of the physical solution method, it is possible to predict the performance indicator (minimization of filling time of resin impregnation along with the porous domain) for each configuration studied. After Step 6, it is necessary to define if the design should be optimized or not.

If the problem is not optimized, a geometrical evaluation is performed, seeking to understand the effect of degrees of freedom over performance indicator, simulating the total number of cases defined. However, if the problem is optimized, it is necessary to specify an optimization method. Here, exhaustive search, which consists of evaluating several geometrical possibilities taking into consideration fixed increments of variation for each degree of freedom (as depicted in Figure 3) for the T-shaped case.

Constructal Design Method

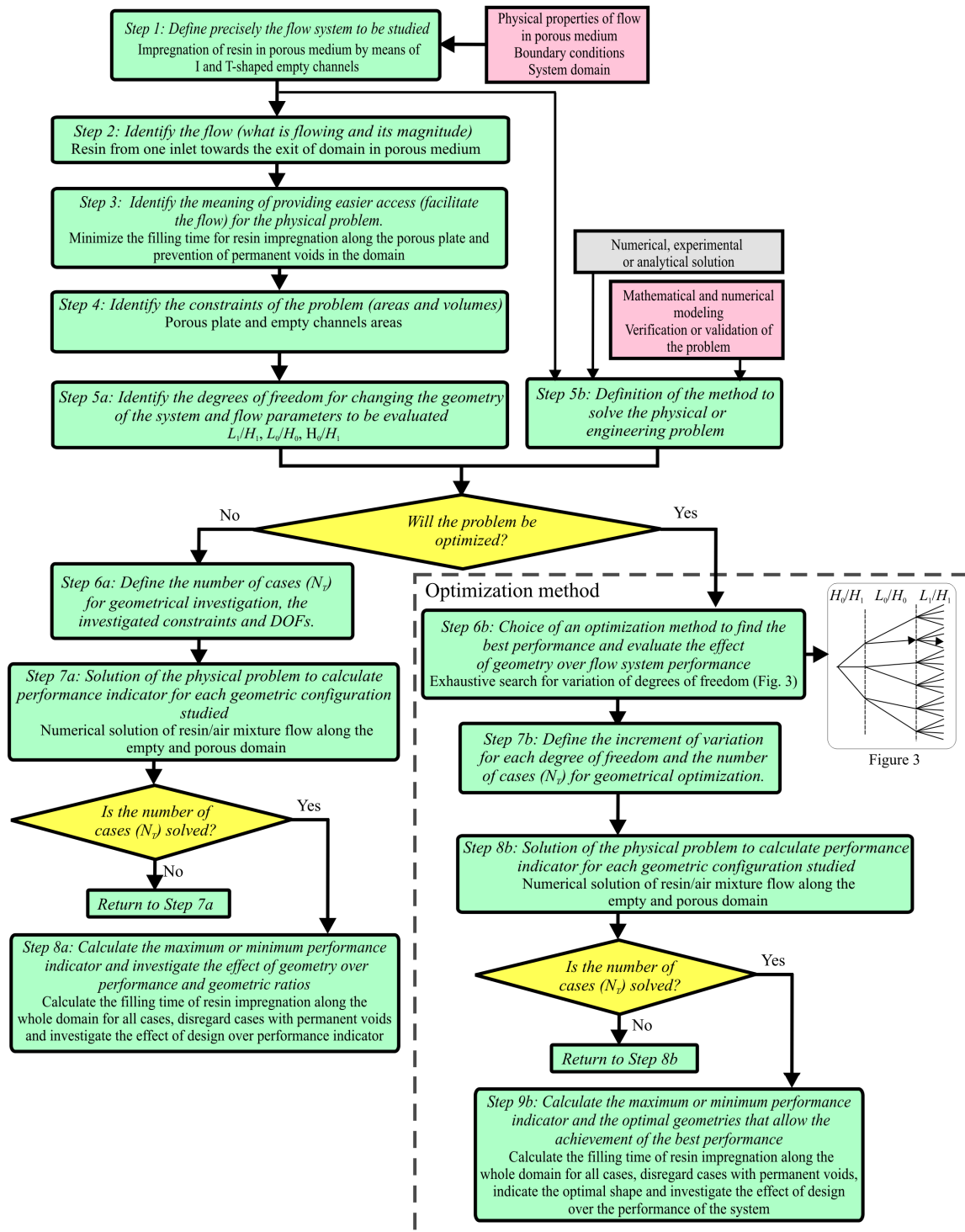


Figure 2. Flow chart illustrating the main steps of the geometrical optimization of I and T-shaped empty channels inserted into the rectangular porous plate for resin impregnation along the domain.

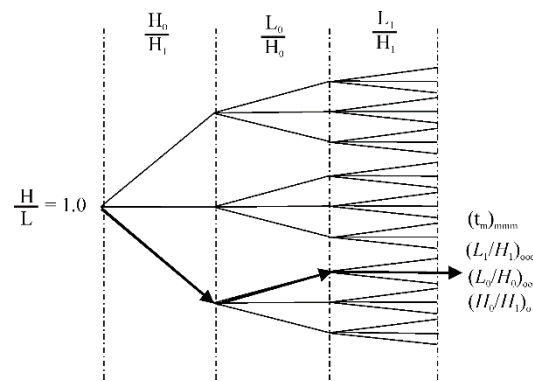


Figure 3. Flowchart of the performed simulations in geometric evaluation of the T-shaped empty channel in resin infusion simulation.

For complete optimization, Steps 6b to 9b, illustrated in Figure 2, are executed. It should be emphasized that heuristic-based optimization methods, e.g., genetic algorithm and simulated annealing, have also been associated with constructal design [48]. These kinds of tools are more used in software packages such as FLUENT [41] and Magma⁵ [49].

These methods required a significantly lower number of cases to be solved, but need verification with exhaustive search for suitable reproduction of the effects of DOFs over the performance indicator.

Each case under analysis is submitted to two restrictions, the total area of the computational domain:

$$A = HL \tag{8}$$

and the area of the empty channel, which for I-shaped and T-shaped channels, respectively, are represented by:

$$A_I = H_0L_0 \tag{9}$$

$$A_T = H_0L_0 + H_1L_1 \tag{10}$$

The dimensions of the external domain with porous medium are: $H = L = 0.5$ m for all simulations, i.e., the outer area is a geometric constraint of the problem, and $H/L = 1.0$ is taken into account. It should be noted that a spacing of 0.05 m was taken into consideration for the sides of the fibrous reinforcement mold, and an additional height of 0.25 m was inserted to prevent void regions in the locality defined by the dashed line shown in Figure 1a,b, which is the main analysis region of this study. The areas A_I and A_T can be represented by the ratio between the empty channel and plate areas (fraction area), written by:

$$\phi = \frac{A_I}{A} = \frac{A_T}{A} \tag{11}$$

For the I-shaped empty channel, one degree of freedom (L_0/H_0) is considered, whereas the T-shaped empty channel has three degrees of freedom (L_0/H_0 , H_0/H_1 , and L_1/H_1). To optimize the geometry of the I-shaped channels, a set of 60 simulations were performed with different L_0/H_0 ratios and different values of ϕ , where $\phi = 0.005; 0.01; 0.03; 0.05$, and 0.1. In the case of T-shaped channels, only $\phi = 0.05$ was evaluated, due to the high number of simulations required for each magnitude of ϕ . In this specific case, a total of 189 simulations were performed. For this case (T-shaped channel), the optimization process was divided into three steps, as shown in Figure 3.

Figure 3 illustrates that in the first optimization step, the ratio L_1/H_1 is varied, while the remaining parameters (L_0/H_0 and H_0/H_1) are kept fixed. To clarify how the terms are assigned, note that the minimum value found for the filling time is named the once minimized filling time (t_m), and the corresponding ratio L_1/H_1 is called the once-optimized ratio of L_1/H_1 , $(L_1/H_1)_o$. In a second step, the same process is repeated by varying L_1/H_1 for the other ratios of L_0/H_0 and maintaining H_0/H_1 constant. At this stage of the process, two degrees of freedom are optimized (L_1/H_1 and L_0/H_0). In this

case, the minimum filling time obtained is twice minimized (t_{mm}), the L_1/H_1 ratio is the twice-optimized ratio $(L_1/H_1)_{oo}$, and the L_0/H_0 ratio is once optimized $(L_0/H_0)_o$. Finally, the second step is repeated for the different ratios of H_0/H_1 evaluated. Thus, the minimum filling time is the thrice-minimized (t_{mmm}), and the optimal shapes are the thrice-optimized ratio of L_1/H_1 , $(L_1/H_1)_{ooo}$, the twice optimized ratio of L_0/H_0 , $(L_0/H_0)_{oo}$, and the once-optimized ratio of H_0/H_1 , $(H_0/H_1)_o$, completing the geometric optimization process.

3. Numerical Modeling and Code Validation

For simulation of the infusion process, the conservation equations of mass, momentum, and transport equation of volume fraction were solved using a commercial CFD (computational fluid dynamics) code based on FVM [39–41]. Numerical simulations were carried out using computers with 4 Intel Xeon processors and 8 threads of 3.30 GHz clock and 8.0 Gb of RAM. In all the simulations, the second-order upwind discretization scheme was used for the treatment of the advective terms. For pressure interpolation, the PRESTO scheme was used. Pressure-velocity coupling was performed with the PISO method, while the Geo-Reconstruction method was used to reconstruct the interface between the two fluids. In addition, sub-relaxation factors of 0.3 and 0.7 are imposed for the conservation equations of mass and momentum, respectively. The simulations are considered converged when the residuals of conservation equations of mass and momentum are lower than $R < 10^{-6}$.

For time discretization, a study of time step independence was performed, since a transient problem was being investigated. Five simulations were performed with a varying time step, and its influence over the volume of domain completely impregnated by the resin was investigated, i.e., the volume of domain with volume fraction of $f = 1.0$. For all simulations, the volume of resin injected up to time of $t = 7.0$ s was evaluated. Table 1 shows, for the analyzed injection time, the volume percentage of the domain filled with resin and the processing time required to carry out the simulations. The analyzed case consists of a I-shaped empty channel with area fraction of $\phi = 0.05$, $H/L = 1.0$ and $L_0/H_0 = 4.0$. It is possible to observe that for values of $\Delta t \leq 1.0 \times 10^{-3}$ s, all employed time steps lead to identical results. For the values of $\Delta t = 1.0 \times 10^{-2}$ s and $\Delta t = 1.0 \times 10^{-1}$ s, there is no convergence in the simulations. Consequently, the time step of $\Delta t = 1.0 \times 10^{-3}$ s is adopted in subsequent geometric evaluation simulations, as it leads to a lower computational effort compared to smaller time steps.

Table 1. Study of sensibility of time step over resin impregnation for an I-shaped empty channel with $\phi = 0.05$, $H/L = 1$, and $L_0/H_0 = 4$.

Time Step (s)	Mold Filling (%)	Processing Time (s)
1.0×10^{-5}	27.1596	171,000
1.0×10^{-4}	27.1596	8900
1.0×10^{-3}	27.1596	1200
1.0×10^{-2} *	—	—
1.0×10^{-1} *	—	—

* Non-converging solutions.

For spatial discretization, the domain was divided into finite rectangular volumes, and a mesh independence test was performed to define the number of volumes used for the simulations. The time step used is defined in Table 1 ($\Delta t = 1.0 \times 10^{-3}$ s). Table 2 shows the number of volumes, the filling time for complete impregnation of resin in the mold, and the processing time required to perform the simulations for each evaluated mesh and for the same I-shaped channel studied in the time independence study, i.e., $\phi = 0.05$, $H/L = 1.0$ and $L_0/H_0 = 4.0$. The following equation presents the criterion for achievement of an independent mesh:

$$Difference = \frac{100 \cdot |t^j - t^{j+1}|}{t^j} < 1.0\% \tag{12}$$

where t^j represents the minimum value of the filling time calculated with the coarser mesh, and t^{j+1} corresponds to the magnitude calculated with the refined successive mesh. Successive refinements determine appropriate mesh size until the magnitude of the difference variable for two successive meshes is lower than 1.0%. In this sense, a mesh with 18,271 finite rectangular volumes is used in this study.

Table 2. Mesh independence test considering an I-shaped empty channel with $\phi = 0.05$, $H/L = 1.0$ and $L_0/H_0 = 4.0$.

Number of Volumes	Filling Time (s)	Difference (%)	Processing Time (s)
1209	188.3	1.69	43,000
4636	185.1	1.18	78,400
18,271	182.9	0.87	126,500
72,451	181.3	—	184,900

To show the reliability of the present computational model, a verification of the numerical method used here was done by comparing the present numerical solution and a classical analytical solution for the rectilinear case. More precisely, resin advancement as a function of infusion time obtained with the present method and the analytical solution described in Jinlian et al. [50] and Rudd [45] are compared. This comparison can be made for empty channels that lead to rectilinear behavior of resin in the porous medium. For the sake of comparison, a simulation in an I-shaped empty channel with $\phi = 0.05$, $H/L = 1.0$, and $L_0/H_0 = 19.0$, where L_0 is equal to L , is chosen. The case with these configurations represents a rectilinear case.

An analytical solution for front-line resin advancement as a function of time is given by [50]:

$$X_f = \sqrt{\frac{2KP_{in}t}{\mu\varepsilon}} \quad (13)$$

where X_f is the position of the resin front-line (m), t is the time (s), μ is the resin viscosity (Pa/s), ε is the porosity, K is the permeability (m^2), and P_{in} is the injection pressure (Pa). It should be noted that the present formulation is only applicable to a constant P_0 situation.

A monitoring line was created in the center of the domain to obtain the numerical results. More precisely, a line that overlaps the y -axis was defined by the following points: P_1 ($x_1 = 0.0$ m, $y_1 = 0.0256$ m) and P_2 ($x_2 = 0.0$ m, $y_2 = 0.7500$ m). The coordinates $x_1 = x_2$ represent the center of the domain in the x -direction, while the coordinate y_1 represents the interface placement between the open channel and the porous medium, and y_2 is the exit region of the resin. Figure 4 shows the advancement of the resin front line as a function of the injection time for both solutions (analytical and numerical) and an illustration of the simulated domain with monitoring points for resin advancement in the porous medium. A maximum difference of 0.66% was observed between the analytical and numerical results, which is an indication of very good agreement. Therefore, the verification of the numerical model presented was satisfactorily achieved, and the code can be used for theoretical recommendations on the geometric configurations of I and T-shaped empty channels inserted in a rectangular porous plate.

It is also worth mentioning that the present computational model was previously verified and validated in the work by the authors of [9]. The resin propagation obtained with this computational model was verified with the analytical data for linear and radial cases and with numerical results obtained with the PAM-RTM[®] software for three-dimensional resin flow in a rectangular box and spherical shell. Moreover, the code was validated with the experimental results obtained by Schmidt et al. [51] for a case of resin flow in a cavity mold with an inlet nozzle. More precisely, it was compared to the results of resin flow advancement as a function of time: differences of nearly 8.0% were found. The cases in Reference [9] mimic resin transfer molding (RTM) or light-resin transfer molding (LRTM) processes. In spite of the simulation of different processes, the fluid dynamic behavior of the resin flow of Reference [9] is the same as performed here. These results were reproduced for

code validation in this study, but are not provided here since they have already been presented in Reference [9].

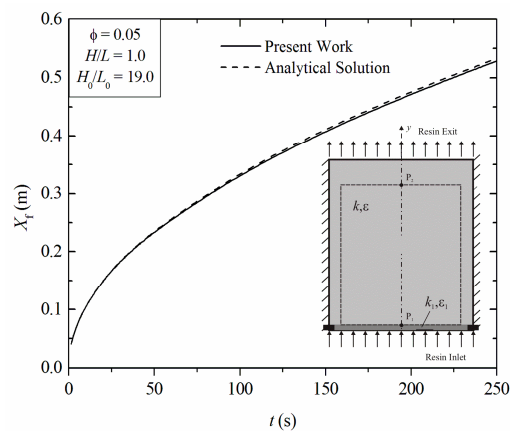


Figure 4. Comparison between the placement of resin flow as a function of time by analytical solution.

4. Results and Discussion

To eliminate residual air from a porous medium, it is necessary to perform successful molding. The formation of voids due to partial impregnation of resin inside the fibrous reinforcement can lead to failures in the use of the final product [45]. In this sense, geometric optimization is essential because it not only increases productivity by reducing the time of injection, but also enhances the quality of the pieces produced. Thus, the prevention of the formation of voids in the porous medium is a restriction in the analysis and definition of the liquid resin infusion (LRI) process.

A reference line was created in the domain to measure filling time (see the horizontal dashed lines in Figure 1a,b, defined by the following points: $P_1 (x_1 = -0.25 \text{ m}, y_1 = 0.50 \text{ m})$ and $P_2 (x_2 = 0.25 \text{ m}, y_2 = 0.50 \text{ m})$). The position of the front line of the resin flow is monitored along this line. When the resin flow completely crosses the reference line, i.e., when the volumetric fraction along the entire line is equal to $f = 1.0$, the infusion process is considered complete.

To evaluate the geometric influence of the I-shaped empty channel over the filling infusion time of the resin along the rectangular porous plate, the fraction area inside the domain is analyzed. Simulations performed with different L_0/H_0 ratios are used to determine the case with lower infusion time for five different fraction areas of the empty channel, $\phi = 0.005; 0.01; 0.03; 0.05$ and 0.1 . It has been found that the effect of the ratio L_0/H_0 over filling time (t) is similar for all investigated fractions ϕ . The only exception happened for $\phi = 0.1$ due to the restriction of the geometry in the upper limit of L_0/H_0 , as can be seen in Figure 5. In general, it is noticed that the lowest L_0/H_0 ratios lead to the best results, i.e., there is a reduction in filling time (t) when the channel has higher penetration in the y -direction of the domain. However, the progressive increase of L_0/H_0 to the upper limit results in a decrease in injection time too. Thus, there is a globally optimized ratio placed in the lowest region of L_0/H_0 and a local optimized ratio region, placed in the superior limit of the ratio L_0/H_0 investigated. The worst performance, for almost all cases of ϕ , is reached for intermediate ratios of L_0/H_0 . Different behavior is noticed only for $\phi = 0.100$, where there is an almost asymptotic growth of filling time as a function of ratio L_0/H_0 , showing that restriction influences the best shape and effect of geometry over the performance indicator.

The results also showed that the best configurations for lower magnitudes of ϕ can have a superior performance than those achieved for intermediate ratios of L_0/H_0 , even for higher magnitudes of ϕ . For example, the best configuration obtained for $\phi = 0.01$, $(L_0/H_0)_o = 0.015$ led to a filling time of $t_m = 105.3 \text{ s}$, which is lower than the filling time reached for several configurations (not optimized) with $\phi = 0.03; 0.05$ and 0.1 . This behavior indicates that geometric rationalization can lead to smaller

dimension channels for a performance superior to that reached for larger channels, where geometric configuration is not optimized.

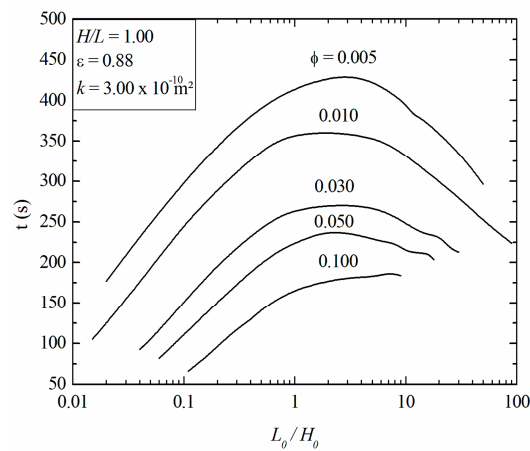


Figure 5. Effect of the L_0/H_0 ratio over resin infusion filling time for different area fractions of the I-shaped empty channels.

The optimal results obtained in Figure 5 for each fraction area, ϕ , are compiled in Figure 6a. Figure 6a shows the influence of the ratio between the channel area and the area of the plate (ϕ) on the once minimized filling time (t_m) for the I-shaped empty channel. Results in Figure 6a indicate that for the largest area fractions (ϕ) of the I-shaped channel, the filling time once minimized (t_m) increases. Figure 6b shows the influence of ϕ on the optimal ratio of L_0/H_0 named $(L_0/H_0)_o$. It is also noted that the behavior of the geometric ratio $(L_0/H_0)_o$ is modified with the variation of the area occupied by the channel, i.e., there is no universal optimal geometry that leads to the best performance for all area fractions of the open channels.

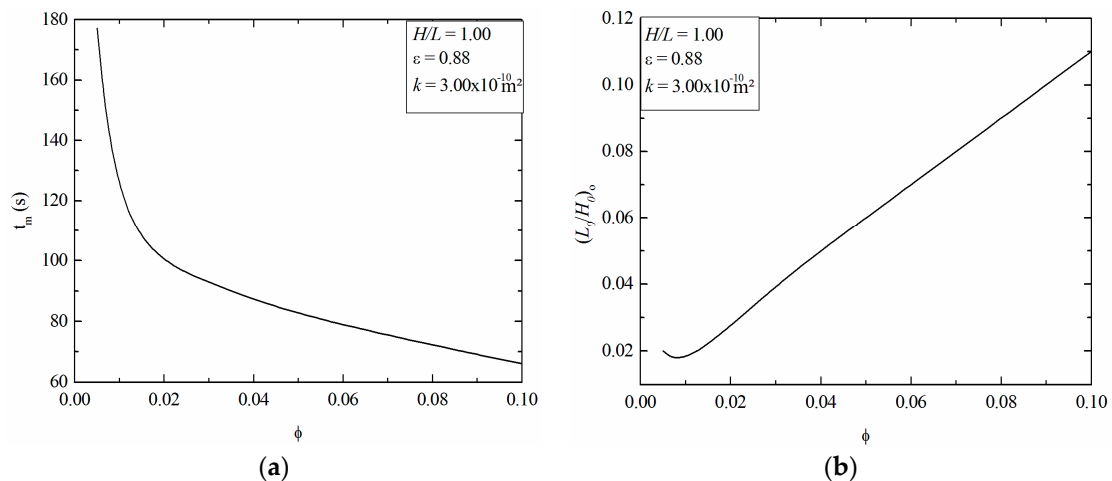


Figure 6. Effect of empty I-shaped channel area fraction (ϕ) over: (a) once minimized filling time (t_m), (b) once optimized L_0/H_0 ratio, $(L_0/H_0)_o$.

To illustrate the influence of ϕ and the L_0/H_0 ratio over resin flow considering the I-shaped channel, Figures 7 and 8 show the behavior of the resin advancement for three different instants of time at $\phi = 0.01$ and 0.1 , respectively. The red region represents the resin, i.e., when the volume fraction is $f = 1.0$, while the blue region represents the air ($f = 0$). Regions with different colors represent resin/air mixture with intermediary volume fractions between resin and air ($0.0 < f < 1.0$). It is worth

mentioning that this description is applied to all figures where the resin volume fraction is illustrated. Channel configuration is illustrated with the black line.

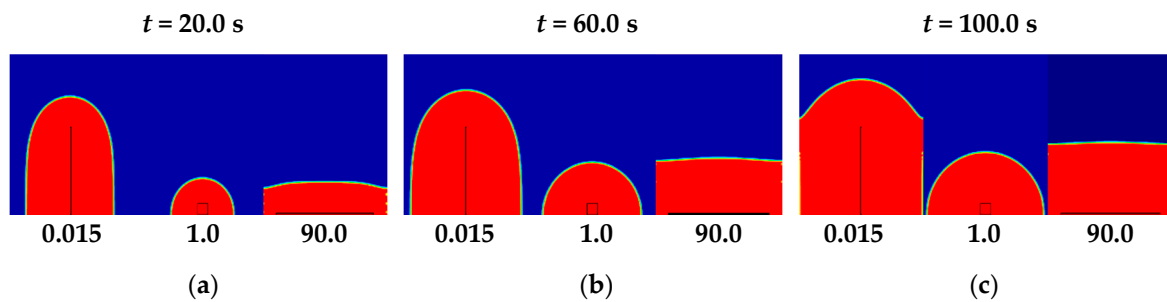


Figure 7. Resin volume fraction for $\phi = 0.01$ and three different ratios of L_0/H_0 : $(L_0/H_0)_o = 0.015$, $L_0/H_0 = 2.0$, $L_0/H_0 = 90.0$ as a function of time: (a) $t = 20.0$ s, (b) $t = 60.0$ s, (c) $t = 100.0$ s.

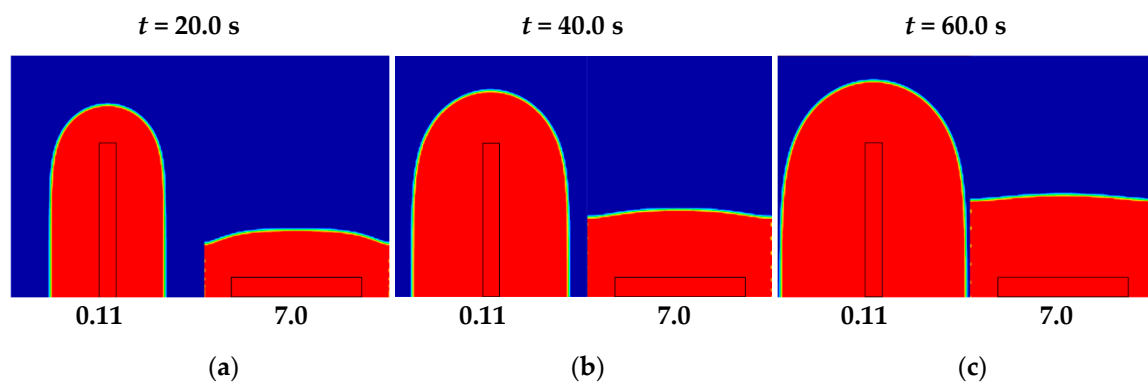


Figure 8. Resin volume fraction for $\phi = 0.1$ and two different ratios of L_0/H_0 : $(L_0/H_0)_o = 0.11$ (optimal), $L_0/H_0 = 7.0$ (worst scenario) as a function of time: (a) $t = 20.0$ s, (b) $t = 40.0$ s, (c) $t = 60.0$ s.

Figure 7 shows resin advancement for $\phi = 0.010$ and three different magnitudes of the ratio L_0/H_0 : $(L_0/H_0)_o = 0.015$, $L_0/H_0 = 1.0$ and $L_0/H_0 = 90.0$, which represents the two extreme magnitudes and an intermediate value of the ratio L_0/H_0 , where the worst performance was reached. Three different instants of time are illustrated to show resin impregnation along time $t = 20.0$ s (Figure 7a); 60.0 s (Figure 7b) and 100.0 s (Figure 7c). Figure 8 shows the resin flows for $\phi = 0.100$ and two different ratios of L_0/H_0 : $(L_0/H_0)_o = 0.11$ and $L_0/H_0 = 7.0$, representing the optimal geometry and worst case for three different instants of time: $t = 20.0$ s (Figure 8a), 40.0 s (Figure 8b), and 60.0 s (Figure 8c).

Results of Figures 7 and 8 indicated that for the smallest ratios of L_0/H_0 , there is a higher advancement of resin in the y -direction. After the spread of resin along the entire empty channel, resin flows from the central region of the domain towards the lateral surfaces of the porous plate. Furthermore, in the superior region of the empty channel, the behavior of the resin flow is similar to that found in radial configurations. This behavior makes the distribution of the resin in the fibrous medium more efficient, minimizing resin filling time in the porous medium. It is also noticed that there are no void formations that could delay the infusion process or cause problems in the manufacturing process. For the highest magnitudes of L_0/H_0 , the channel is placed in the lower region of the porous plate, leading to an almost constant front-line of resin.

Moreover, resin advances towards the exit of the porous domain with a behavior similar to the rectilinear case. In a general sense, geometrical investigation of I-shaped empty channels has attested that the elongated channels in resin propagation direction led to the best performance due to the increase of pressure gradient imposed inside the mold. This behavior is in agreement with the constructal principle of the optimal distribution of imperfections.

Subsequent investigation consisted of the evaluation of the influence of the T-shaped channel aspect ratios L_1/H_1 , L_0/H_0 , and H_0/H_1 on the filling time for resin impregnation in the rectangular

porous plate. For this configuration, the optimization process was performed only for $\phi = 0.05$ due to the high number of simulations needed. Firstly, the effect of the ratio L_1/H_1 on resin infusion time along the mold was evaluated for different values of the ratio L_0/H_0 , keeping H_0/H_1 fixed. Figure 9a–d present the effect of the ratio L_1/H_1 over the filling time for various constant ratios of L_0/H_0 and four different magnitudes of $H_0/H_1 = 10.0, 20.0, 30.0$ and 40.0 , respectively. It should be noted that for $H_0/H_1 = 30.0$ and $H_0/H_1 = 40.0$, the L_0/H_0 search space becomes more restricted due to the generation of very thin channels. For example, when $H_0/H_1 = 40.0$, the variation is viable only in the range $0.05 \leq L_0/H_0 \leq 0.1$ because for higher magnitudes of L_1/H_1 , the thickness of the bifurcated channel would become insignificant, which disfigures the T-shaped geometry of the channel and leads to the generation of permanent voids.

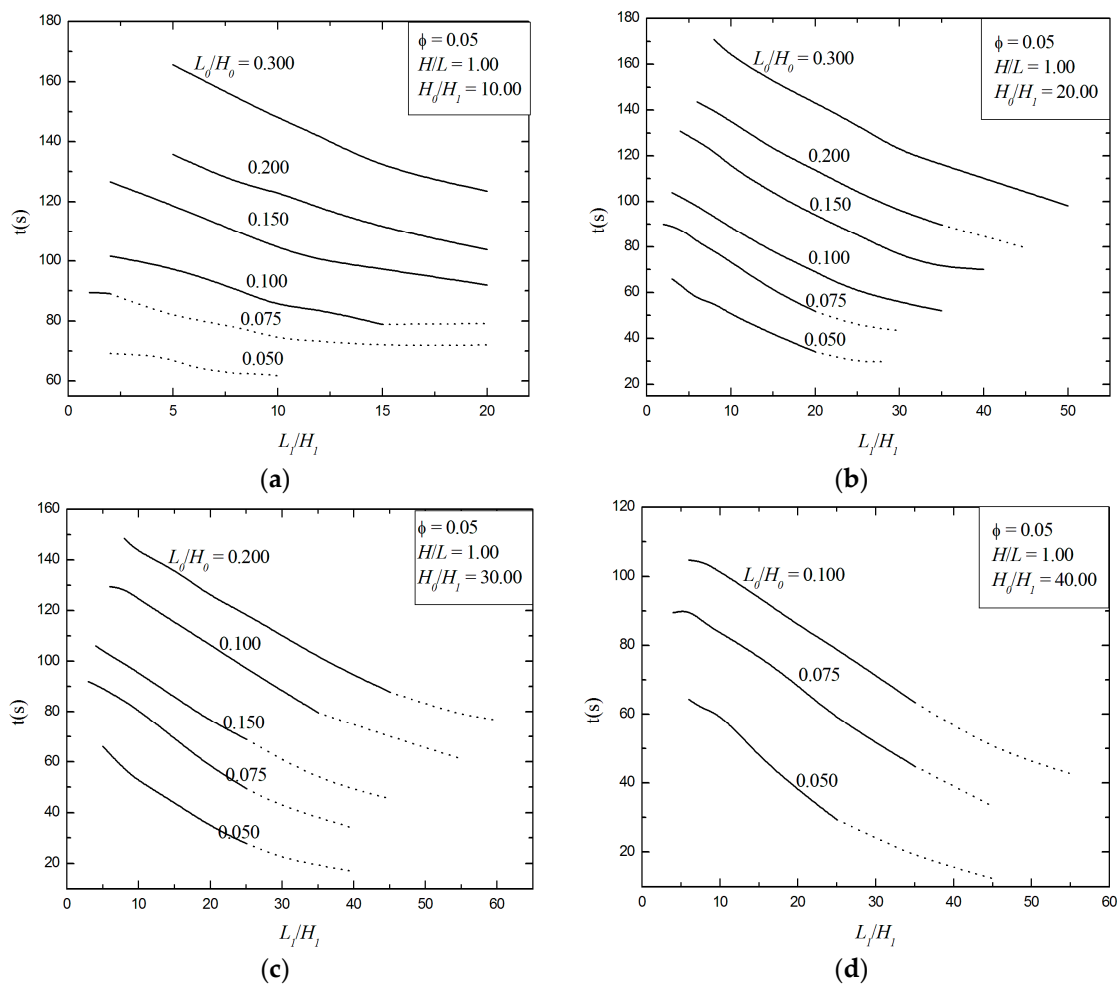


Figure 9. Effect of ratio L_1/H_1 over resin infusion filling time for several values of ratio L_0/H_0 and fixed values of H_0/H_1 : (a) $H_0/H_1 = 10.0$, (b) $H_0/H_1 = 20.0$, (c) $H_0/H_1 = 30.0$, (d) $H_0/H_1 = 40.0$.

In Figure 9a–d, the continuous curves represent valid geometries, i.e., those geometries with no permanent void inside the porous plate or empty channel. The dashed curves represent cases where permanent voids are generated, even if the monitoring line indicates complete impregnation of the mold (with $f = 1.0$ along the whole measurement line). In this sense, these results are disregarded for optimization evaluation, since void formations are a critical problem in manufacturing. It is to be noted that some cases in the dashed region of the curves achieved lower filling times, indicating that the resin has a higher impregnation in the porous plate. However, the mold was not completely filled.

Results in Figure 9a–d also show that the higher magnitudes of L_1/H_1 for all investigated ratios of L_0/H_0 lead to the best performance, i.e., there is a reduction in resin filling time (t) when the bifurcated

channel has higher penetration into the mold toward its lateral surfaces. However, some T-shaped channels with higher ratios of L_1/H_1 and lower magnitudes of L_0/H_0 lead to the formation of permanent voids, mainly when the geometry is composed of skinny channels. Therefore, the results recommend the building of elongated channels, since this does not lead to skinny channels. The generation of permanent voids occur, in general, in the corner that connects the single stem to the bifurcated branches. One possible reason for this behavior is the detachment of resin flow in the channel corner with not enough resin flow coming from the inlet to degenerate the void. Therefore, the permanent void remains during all the simulations in the area mentioned above.

To illustrate the influence of ratio L_1/H_1 on mold filling time, Figure 10 shows the advancement of resin for two different ratios of L_1/H_1 , $L_1/H_1 = 6.0$ and $(L_1/H_1)_o = 35.0$, which represents the worst and best shapes when the constant ratios of $H_0/H_1 = 40.0$ and $L_0/H_0 = 0.1$ are assumed. For both cases, the volume fraction fields for three different instants of time— $t = 10.0$ s, 30.0 s, and 60.0 s—are presented in Figure 10a–c, respectively. For $L_1/H_1 = 6.0$, filling time of $t = 104.7$ s is obtained, while the ratio $(L_1/H_1)_o = 35.0$ leads to a resin injection time of the once minimized of $t_m = 63.5$ s, which is about 65.0% faster than the worst-performing geometry. For the lower magnitudes of H_1/L_1 , resin distribution occurs in a radial form in the upper region of the T-shaped channel and linearly from the center to the side surfaces of the mold at the bottom region of the T-shaped channel. This behavior is quite similar to that seen for I-shaped empty channels with high intrusion in the porous plate. As the ratio of H_1/L_1 is changed to $(H_1/L_1)_o = 35.0$, the radial advancement of the resin at the upper region of the T-shaped channel is found to be intensified, when compared with the previous case ($H_1/L_1 = 6.0$). This effect also intensifies the linear advancement of resin in the inferior region of the porous plate.

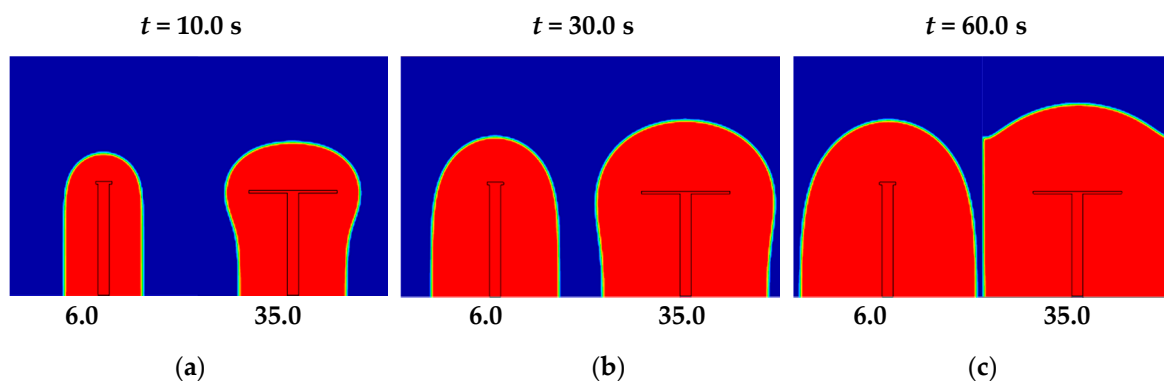


Figure 10. Resin volume fraction for $\phi = 0.05$, $H/L = 1.0$, $H_0/H_1 = 40.0$, $L_0/H_0 = 0.1$ and two different ratios of $L_1/H_1 = 6.0$ and $(L_1/H_1)_o = 35.0$ as a function of time: (a) $t = 10.0$ s, (b) $t = 30.0$ s, (c) $t = 60.0$ s.

Consequently, the filling of the resin in the horizontal direction (from the open channel towards the side walls) is completed in a shorter amount of time, also leading to an improvement in resin advancement towards the porous plate exit. However, significant increase in bifurcated length (augmentation of the ratio H_1/L_1) leads to the formation of permanent voids inside the plate. It is worth mentioning that the channel area is constant; as a consequence, augmentation of the channel bifurcated branch leads to a decrease in channel thickness, which is the main factor responsible for the formation of voids, especially in the corners between the single and bifurcated regions of the channel.

The variation of the L_1/H_1 ratio provides the once minimized filling time (t_m) of the resin in the porous plate for each investigated ratio of L_0/H_0 and different ratios of H_0/H_1 . In the second optimization level, the results of Figure 9 are compiled and presented in Figure 11a,b.

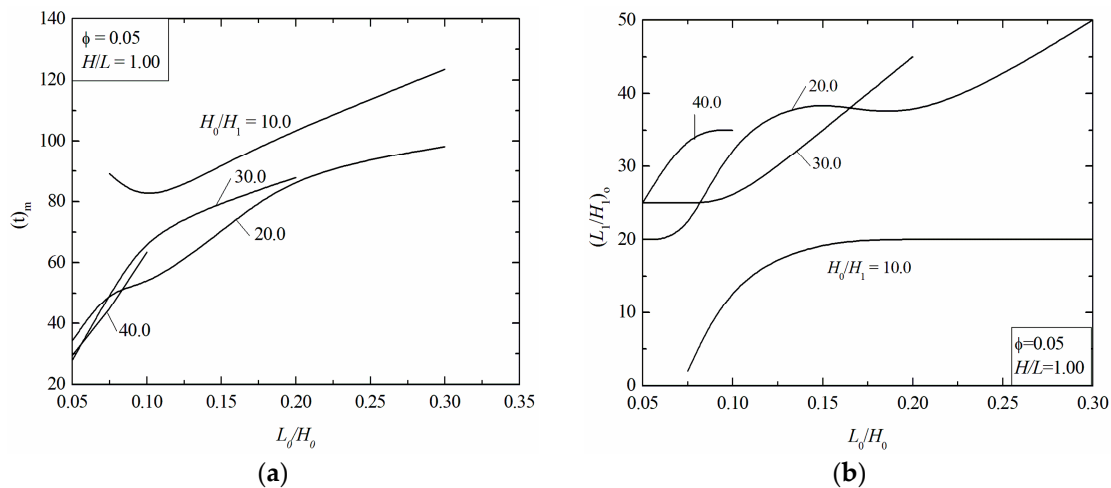


Figure 11. Effect of the ratio L_0/H_0 for different ratios of H_0/H_1 on (a) infusion time (once minimized), $(t)_m$; (b) ratio (once optimized), $(L_1/H_1)_o$.

Figure 11a illustrates the influence of the ratio L_0/H_0 over the once minimized filling time, t_m , for different H_0/H_1 ratios studied here. It can be noted that for $H_0/H_1 = 20.0; 30.0$ and 40.0 , the effect of the L_0/H_0 over t_m is similar, except for cases with $H_0/H_1 = 10.0$. In general, it is noticed that lower ratios of L_0/H_0 present a predominance in achieving the twice-minimized filling time (t_{mm}), i.e., the best shapes are obtained when the main channel has a higher penetration in the direction of the exit region of the domain. For the ratio $H_0/H_1 = 10.0$, it can be observed that intermediate ratios of L_0/H_0 lead to the best performance of the problem. For the lowest magnitudes of L_0/H_0 , the optimal ratios of $(L_1/H_1)_o$ suffer a strong decrease (see Figure 11b), degenerating the T-shaped channel into an I-shaped one. For higher magnitudes of L_0/H_0 , the T-shaped channel is strongly restricted in the lower region of the porous plate. Figure 11b highlights the influence of the ratio L_0/H_0 over the once-optimized ratio of L_1/H_1 , $(L_1/H_1)_o$, for the four different magnitudes of H_0/H_1 investigated. The effect of L_0/H_0 over $(L_1/H_1)_o$ varied for different magnitudes of H_0/H_1 . For the ratios $H_0/H_1 = 20.0; 30.0$ and 40.0 , the best shapes are obtained for $(L_0/H_0)_o = 0.05$ and for high magnitudes of $(L_1/H_1)_{oo}$ in the range $20.0 \leq (L_1/H_1)_{oo} \leq 25.0$, corroborating previous findings that the best performance is achieved for the most elongated possible single and bifurcated branches of T-shaped channel. For $H_0/H_1 = 10.0$, the best configurations changed for $(L_0/H_0)_o = 0.075$ and the optimal ratio $(L_1/H_1)_{oo}$ dropped dramatically to $(L_1/H_1)_{oo} = 2.0$. In general, the results show that changes in one degree of freedom have a strong influence on the effect of other geometric ratios on the performance indicator. In this case, it was also noticed that there is no optimal universal configuration that leads to the best performance in this problem.

The last optimization step consists of investigation on the influence of the ratio H_0/H_1 over the twice-minimized filling time (t_{mm}) and the respective optimal configurations: $(L_0/H_0)_o$ and $(L_1/H_1)_{oo}$. To obtain this evaluation, the best results achieved in Figure 11a,b are compiled in Figure 12.

These results show that the behavior of the (t_{mm}) is largely affected by ratio H_0/H_1 , and it has a strong dependence on ratios $(L_1/H_1)_{oo}$ and $(L_0/H_0)_o$. The thrice-minimized filling time (t_{mmm}) is obtained for the rate $(H_0/H_1)_o = 30.0$, which is only 5.0% lower than that reached for $H_0/H_1 = 40.0$. In general, it is possible to state that the higher magnitudes of the ratio H_0/H_1 led to the best performance for this problem. The lowest magnitude of $H_0/H_1 = 10.0$ obtained a performance 183.0% inferior to that reached for the optimal ratio $(H_0/H_1)_o = 30.0$. Moreover, differences found for t_{mm} between the ratios $H_0/H_1 = 20.0$ and $(H_0/H_1)_o = 30.0$ was nearly 23.0%.

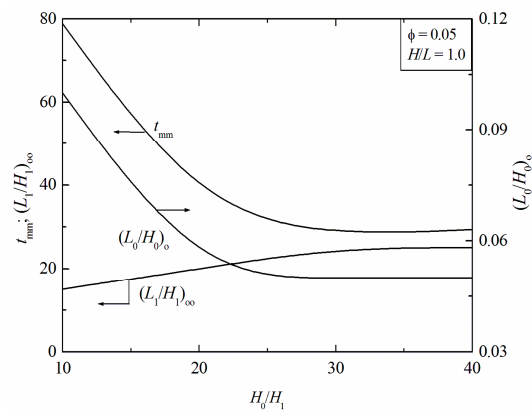


Figure 12. Effect of the ratio H_0/H_1 for twice-minimized infusion time, t_{mm} , and the respective optimal shapes, $(L_0/H_0)_o$, $(L_1/H_1)_{oo}$.

Concerning optimal shapes, it was noticed that the ratio $(L_0/H_0)_o$ suffered a strong decrease in its magnitude in the region $10.0 \leq H_0/H_1 \leq 20.0$, followed by a smooth decrease in the range $20.0 \leq H_0/H_1 \leq 30.0$ and a stabilization for $H_0/H_1 \geq 30.0$. For $(L_1/H_1)_{oo}$, an increase in magnitude was noticed, until stabilization for $H_0/H_1 \geq 30.0$. In general, the results show the importance of geometric investigation in the reduction of filling time of resin impregnation along a porous domain.

To illustrate the transient behavior of resin flow in the mold, Figures 13 and 14 show the distribution of resin volume fraction as a function of time for the worst performing ratio, $H_0/H_1 = 10.0$, and for the optimal ratio $(H_0/H_1)_o = 30.0$, respectively. Topologies are presented for the following times: $t = 20.0$ s; 40.0 s and 60.0 s, respectively. Figure 7, Figure 8, and Figure 10 illustrate the topology of the configuration of the empty channel.

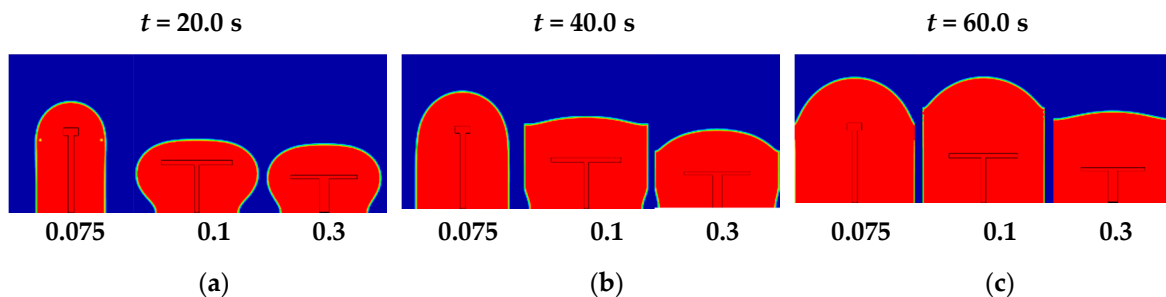


Figure 13. Resin volume fraction for $\phi = 0.05$, $H/L = 1.0$, $H_0/H_1 = 10.0$, for three different ratios of $L_0/H_0 = 0.075$, $(L_0/H_0)_o = 0.100$ and $L_0/H_0 = 0.300$ as a function of time: (a) $t = 20.0$ s, (b) $t = 40.0$ s, (c) $t = 60.0$ s.

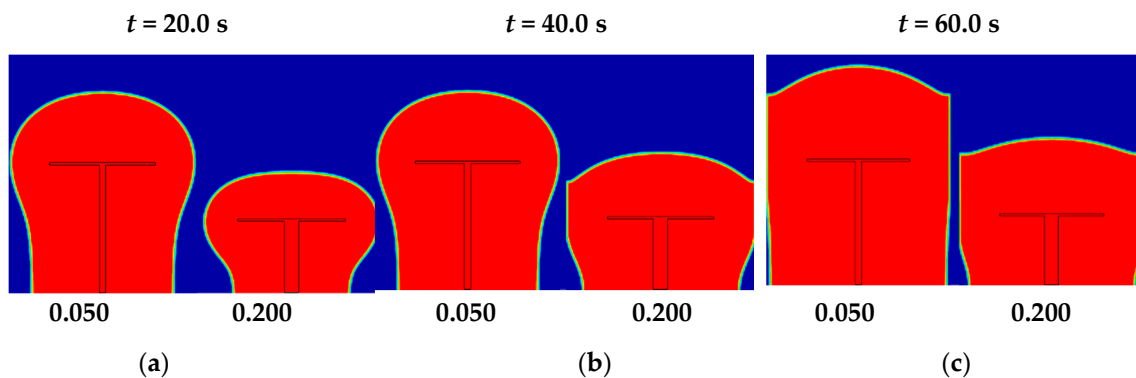


Figure 14. Resin volumetric fraction for $\phi = 0.05$, $H/L = 1.0$, $H_0/H_1 = 30.0$, for two different ratios of $(L_0/H_0)_{oo} = 0.050$ and $L_0/H_0 = 0.200$ as a function of time: (a) $t = 20.0$ s, (b) $t = 40.0$ s, (c) $t = 60.0$ s.

Figure 13 shows resin progression at the analyzed instants of time for $H_0/H_1 = 10.0$ and $L_0/H_0 = 0.075$, $(L_0/H_0)_o = 0.1$, and $L_0/H_0 = 0.3$ corresponds to the lowest ratio of L_0/H_0 , the optimal configuration, and the superior magnitude, respectively. For the lowest ratio of L_0/H_0 , it is observed that the T-shaped channel almost degenerates into an I-shaped channel. This configuration leads to a poor distribution of resin in the lower region of the porous plate. The resin propagation is shown for three different instants of time: $t = 20.0$ s (Figure 13a), $t = 40.0$ s (Figure 13b) and $t = 60.0$ s (Figure 13c).

For optimal configuration, despite the T-shaped channel being placed in a lower region of the porous plate in comparison with the case with $L_0/H_0 = 0.075$, the elongated bifurcated branches led to better distribution of the resin in the lower region of the porous plate and allow easy resin propagation towards the exit of the domain. For the superior ratio of $L_0/H_0 = 0.3$, the restriction of the T-shaped channel in the lower region of the porous plate affects the advancement of resin towards the exit of the domain, leading to a poorer performance than the optimal ratio of L_0/H_0 .

Figure 14 presents the results of resin spread for the optimum ratio of H_0/H_1 , $(H_0/H_1)_o = 30.0$, for two different ratios of L_0/H_0 , $(L_0/H_0)_{oo} = 0.05$, $L_0/H_0 = 0.2$ and three different instants of time: $t = 20.0$ s (Figure 14a), $t = 40.0$ s (Figure 14b), $t = 60.0$ s (Figure 14c). These ratios represent the corresponding twice-optimized and worst-case scenarios for the ratio of $(H_0/H_1)_o = 30.0$, respectively. For the ratio $(L_0/H_0)_{oo} = 0.05$, an injection time of $t_{mmm} = 27.9$ s is obtained, and the ratio $L_0/H_0 = 0.2$ leads to a once minimized injection time of $t_m = 87.9$ s, which is, about of 215.0% higher than the previously obtained optimal geometry. It is then possible to significantly improve the performance of the studied system even in the last level of optimization.

In a general sense, the results demonstrate that for the T-shaped channel, all geometrical ratios (degrees of freedom) affect the filling time of resin impregnation in a porous domain. They also show that one degree of freedom has a strong influence over the optimal ratios of other geometric ratios, e.g., the ratio H_0/H_1 affected the optimal ratios of $(L_1/H_1)_{oo}$ and $(L_0/H_0)_o$.

All the geometrical parameters studied here (L_1/H_1 , L_0/H_0 , and H_0/H_1) has some sensibility in the infusion process and cannot be neglected. Moreover, a comparison between the performance of the T-shaped and I-shaped empty channels, for the same conditions, demonstrates that the thrice-optimized T-shaped channel leads to performance that is almost three times superior to that achieved by the optimal I-shaped configuration.

In the present fluid dynamic conditions, where resin flow has little advective dominance, the rectangular porous plate can be viewed as an elementary construction of multiple structures generated by the replication of a porous plate in x - or y -axes. In this case, multiple optimal configurations of I and T-shaped channels can be associated in a series and/or parallel using the optimal configurations reached in this work.

5. Conclusions

This paper developed a numerical study of the geometric evaluation of empty channels inserted in a porous rectangular plate, mimicking the liquid resin infusion process (LRI), and applying constructal design and exhaustive search (ES) for geometric optimization. The primary purposes here were to analyze the influence of the design of I and T-shaped empty channels on the filling time of resin impregnation in a porous plate, preventing the generation of permanent voids.

The following important recommendations were made:

- I-shaped channels with the highest penetration in the y -direction of the porous domain, as well as the highest magnitude of area fraction (ϕ) had a higher performance in minimization of filling time, as expected.
- For the T-shaped channels, the results demonstrated that the best performance was reached for the highest possible penetration of single and bifurcated channels in the porous plate, with the exception of cases with very thin channels that saw the generation of permanent voids.

- The results for the T-shaped channels demonstrated that all studied geometric ratios had sensibility over the performance indicator (filling time) and the optimal ratios. For example, the ratio H_0/H_1 had a strong influence on the twice-minimized filling time (t_{mm}) and the respective optimal ratios, $(L_1/H_1)_{oo}$ and $(L_0/H_0)_o$.
- For the same fluid dynamic conditions, the results indicated that the most complex empty T-shaped channel was beneficial in improving resin flow impregnation in the whole domain of the porous plate, as compared to the elementary I-shaped one.
- In general, the results of this study demonstrated the importance of constructal design in the geometric evaluation of the liquid resin infusion process.

Other geometrical configurations, such as Y-shaped and fishbone empty channels, or geometries being constructed with no pre-defined form are recommended for future studies. Another interesting possibility of study is the insertion of two or more inlet ports investigating the influence of interactions between different channels on their optimal shapes.

Author Contributions: Conceptualization, J.A.S., and E.D.d.S.; methodology, G.M.C.M., L.A.I., and R.d.L.L.; software, G.M.C.M., J.A.S., and E.D.d.S.; validation, L.A.I., C.F., G.M.C.M., and J.A.S.; formal analysis, E.D.d.S., L.A.O.R., J.A.S., and C.F.; investigation, G.M.C.M., E.D.d.S., and J.A.S.; resources, S.C.A., J.A.S., and E.D.d.S.; data curation, E.D.d.S., and J.A.S.; writing—original draft preparation, G.M.C.M., R.d.L.L., and E.D.d.S.; writing—review and editing, E.D.d.S., L.A.I., and C.F.; visualization, J.S. and L.A.O.R.; supervision, G.M.C.M., L.A.O.R., and C.F.; project administration, E.D.d.S. and J.A.S.; funding acquisition, G.M.C.M., J.A.S., and E.D.d.S. All authors have read and agreed to the published version of the manuscript.

Funding: This research was funded by the Brazilian Coordination for the Improvement of Higher Education Personnel (CAPES) (Finance Code 001), the Brazilian National Council for Scientific and Technological Development (CNPq), and the Italian Minister of Foreign Affairs and International Cooperation (MAECI), as part of the ‘Two Seats for a Solar Car’ international project.

Acknowledgments: The authors thank Giangiacomo Minak for supporting this publication.

Conflicts of Interest: The authors declare no conflict of interest. The funders had no role in the design of the study; in the collection, analyses, or interpretation of data; in the writing of the manuscript, or in the decision to publish the results.

Nomenclature

A	Area of the rectangular porous medium, m^2
A_I	Area of the I-shaped empty channel, m^2
A_T	Area of the T-shaped empty channel, m^2
\vec{F}	External forces per unit volume, N/m^3
f	Volume fraction, [-]
H	Height of rectangular porous mold, m
H_0	Length of a single channel, m
H_1	Thickness of the bifurcated channel, m
K	Permeability of the medium, m^2
L	Length of rectangular porous mold, m
L_0	Thickness of the single-channel, m
L_1	Length of the bifurcated channel, m
P	Total pressure, Pa
P_{in}	Injection pressure, Pa
P_{out}	Exit pressure, Pa
t	Time, s
\vec{V}	Velocity vector, m/s
x, y	Spatial coordinates of a two-dimensional domain, m
X_f	Position of the advancement of resin front line in verification case, m

Greek symbols

ρ	Density, kg/m ³
μ	Fluid dynamic viscosity, Pa s
ε	Porosity, [-]
ϕ	The ratio between the empty channel and the porous plate areas, [-]
$\bar{\tau}$	Stress tensor, N/m ²

Subscripts

o	Once optimized
oo	Twice optimized
ooo	Thrice optimized
m	Once minimized
mm	Twice minimized
mmm	Thrice minimized
<i>T</i>	Transposed
0	Single-channel
1	Bifurcated channel

References

1. Wang, P.; Drapier, S.; Molimard, J.; Vautrin, A.; Minni, J. Numerical and experimental analyses of resin infusion manufacturing processes of composite materials. *J. Compos. Mater.* **2012**, *46*, 1617–1631. [[CrossRef](#)]
2. Yang, J.; Jia, Y.; Ding, Y.; He, H.; Shi, T.; An, L. Edge effect in RTM processes under constant pressure injection conditions. *J. Appl. Polym. Sci.* **2010**, *118*, 1014–1019. [[CrossRef](#)]
3. Brouwer, W.D.; van Herpt, E.C.F.C.; Labordus, M. Vacuum injection moulding for large structural applications. *Compos. Part A Appl. Sci. Manuf.* **2003**, *34*, 551–558. [[CrossRef](#)]
4. Goncharova, G.; Cosson, B.; Lagardère, M.D. Analytical modeling of composite manufacturing by vacuum assisted infusion with minimal experimental characterization of random fabrics. *J. Mater. Process. Technol.* **2015**, *219*, 173–180. [[CrossRef](#)]
5. Pierce, R.S.; Falzon, B.G. Simulating resin Infusion through textile reinforcement materials for the manufacture of complex composite structures. *Engineering* **2017**, *3*, 596–607. [[CrossRef](#)]
6. Rondina, F.; Taddia, S.; Mazzocchetti, L.; Donati, L.; Minak, G.; Rosenberg, P.; Bedeschi, A.; Dolcini, E. Development of full carbon wheels for sport cars with high-volume technology. *Compos. Struct.* **2018**, *192*, 368–378. [[CrossRef](#)]
7. Poodts, E.; Minak, G.; Mazzocchetti, L.; Giorgini, L. Fabrication, process simulation and testing of a thick CFRP component using the RTM process. *Compos. Part B Eng.* **2014**, *56*, 673–680. [[CrossRef](#)]
8. Poodts, E.; Minak, G.; Dolcini, E.; Donati, L. FE analysis and production experience of a sandwich structure component manufactured by means of vacuum assisted resin infusion process. *Compos. Part B Eng.* **2013**, *53*, 179–186. [[CrossRef](#)]
9. Isoldi, L.A.; Oliveira, C.P.; Rocha, L.A.O.; Souza, J.A.; Amico, S.C. Three-dimensional numerical modeling of RTM and LRTM processes. *J. Braz. Soc. Mech. Sci. Eng.* **2012**, *34*, 105–111. [[CrossRef](#)]
10. Grössing, H.; Stadlmajer, N.; Fauster, E.; Fleischmann, M.; Schledjewski, R. Flow front advancement during composite processing: Predictions from numerical filling simulation tools in comparison with real-world experiments. *Polym. Compos.* **2016**, *37*, 2782–2793. [[CrossRef](#)]
11. Sirtautas, J.; Pickett, A.K.; George, A. Materials characterization and analysis for flow simulation of liquid resin infusion. *Appl. Compos. Mater.* **2015**, *22*, 323–341. [[CrossRef](#)]
12. Pierce, R.S.; Falzon, B.G.; Thompson, M.C. A multi-physics process model for simulating the manufacture of resin-infused composite aerostructures. *Compos. Sci. Technol.* **2017**, *149*, 269–279. [[CrossRef](#)]
13. Chebil, N.; Deléglise-Lagardère, M.; Park, C.H. Efficient numerical simulation method for three dimensional resin flow in laminated preform during liquid composite molding processes. *Compos. Part A Appl. Sci. Manuf.* **2019**, *125*, 105519. [[CrossRef](#)]
14. Rubino, F.; Carlone, P. A semi-analytical model to predict infusion time and reinforced thickness in VARTM and SCRIMP processes. *Polymers* **2019**, *11*, 20. [[CrossRef](#)]
15. Falaschetti, M.P.; Rondina, F.; Zavatta, N.; Gagnani, L.; Gironi, M.; Troiani, M.; Donati, L. Material Characterization for Reliable Resin Transfer Molding Process Simulation. *Appl. Sci.* **2020**, *10*, 1814. [[CrossRef](#)]

16. Mathur, R.; Advani, S.G.; Fink, B.K. Use of genetic algorithms to optimize gate and vent locations for the resin transfer molding process. *Polym. Compos.* **1999**, *20*, 167–178. [[CrossRef](#)]
17. Jiang, S.; Zhang, C.; Wang, B. A process performance index and its application to optimization of the RTM process. *Polym. Compos.* **2001**, *22*, 690–701. [[CrossRef](#)]
18. Luo, J.; Liang, Z.; Zhang, C.; Wang, B. Optimum tooling design for resin transfer molding with virtual manufacturing and artificial intelligence. *Compos. Part A Appl. Sci. Manuf.* **2001**, *32*, 877–888. [[CrossRef](#)]
19. Ratle, F.; Achim, V.; Trochu, F. Evolutionary operators for optimal gate location in liquid composite moulding. *Appl. Soft Comput.* **2009**, *9*, 817–823. [[CrossRef](#)]
20. Wang, J.; Simacek, P.; Advani, S.G. Use of centroidal Voronoi diagram to find optimal gate locations to minimize mold filling time in resin transfer molding. *Compos. Part A Appl. Sci. Manuf.* **2016**, *87*, 243–255. [[CrossRef](#)]
21. Gomes, P.P.; Ferro, O.A.G.; Rezende, M.C. Experimental characterization and simulation of VARTM process to obtain carbon/epoxy composites. In Proceedings of the 1st Brazilian Conference on Composite Materials (BCCM1), Natal, Brazil, 16–19 July 2012.
22. Struzziero, G.; Skordos, A.A. Multi-objective optimization of resin infusion. *Adv. Manuf. Polym. Compos. Sci.* **2019**, *5*, 17–28. [[CrossRef](#)]
23. Geng, Y.; Jiang, J.; Chen, N. Local impregnation behavior and simulation of non-crimp fabric on curved plates in vacuum assisted resin transfer molding. *Compos. Struct.* **2019**, *208*, 517–524. [[CrossRef](#)]
24. Shevtsov, S.; Zhilyaev, I.; Chang, S.-H.; Wu, J.-K.; Huang, J.-P.; Snezhina, N. Experimental and numerical study of vacuum resin infusion for thin-walled composite parts. *Appl. Sci.* **2020**, *10*, 1485. [[CrossRef](#)]
25. Bejan, A. *Shape and Structure, from Engineering to Nature*; Cambridge University Press: New York, NY, USA, 2000.
26. Bejan, A.; Lorente, S. *Design with Constructal Theory*; John Wiley & Sons: Hoboken, NJ, USA, 2008.
27. Bejan, A.; Zane, P. *Design in Nature, How the Constructal Law Governs Evolution in Biology, Physics, Technology, and Social Organization*, 1st ed.; Doubleday: New York, NY, USA, 2012.
28. Bejan, A. *The Physics of Life, the Evolution of Everything*; St. Martins Press: New York City, NY, USA, 2016.
29. Bejan, A. Thermodynamics today. *Energy* **2018**, *160*, 1208–1219. [[CrossRef](#)]
30. Xie, G.; Song, Y.; Asadi, M.; Lorenzini, G. Optimization of Pin-Fins for a Heat Exchanger by Entropy Generation Minimization and Constructal Law. *J. Heat Transf.* **2015**, *137*, 061901. [[CrossRef](#)]
31. Hajmohammadi, M.R. Introducing a ψ -shaped cavity for cooling a heat generating medium. *Int. J. Therm. Sci.* **2017**, *121*, 204–212. [[CrossRef](#)]
32. Mirzaei, M.; Hajabdollahi, H.; Fadakar, H. Multi-objective optimization of shell-and-tube heat exchanger by constructal theory. *Appl. Therm. Eng.* **2017**, *125*, 9–19. [[CrossRef](#)]
33. Bello-Ochende, T.; Olakoyejo, O.T.; Meyer, J.P.; Bejan, A.; Lorente, S. Constructal flow orientation in conjugate cooling channels with internal heat generation. *Int. J. Heat Mass Transf.* **2013**, *57*, 241–249. [[CrossRef](#)]
34. Martins, J.C.; Goulart, M.M.; Gomes, M.N.; Souza, J.A.; Rocha, L.A.O.; Isoldi, L.A.; dos Santos, E.D. Geometric evaluation of the main operational principle of an overtopping wave energy converter by means of Constructal Design. *Renew. Energy* **2018**, *118*, 727–741. [[CrossRef](#)]
35. Feng, H.; Chen, L.; Xie, Z. Multi-disciplinary, multi-objective and multi-scale constructal optimizations for heat and mass transfer processes performed in Naval University of Engineering, a review. *Int. J. Heat Mass Transf.* **2017**, *115*, 86–98. [[CrossRef](#)]
36. Bejan, A.; Gunes, U.; Sahin, B. The evolution of air and maritime transport. *Appl. Phys. Rev.* **2019**, *6*, 021319. [[CrossRef](#)]
37. Isoldi, L.A.; Souza, J.A.; dos Santos, E.D.; Marchesini, R.; Porto, J.; Letzow, M.; Rocha, L.A.O.; Amico, S.C. Constructal design applied to the light resin transfer molding (LRTM) manufacturing process. In Proceedings of the 22nd ABCM International Congress of Mechanical Engineering (COBEM), Ribeirao Preto, Brazil, 3–7 November 2013.
38. Magalhães, G.M.C.; Lorenzini, G.; Nardi, M.G.; Amico, S.C.; Isoldi, L.A.; Rocha, L.A.O.; Souza, J.A.; dos Santos, E.D. Geometrical evaluation of a resin infusion process by means of constructal design. *Int. J. Heat Technol.* **2016**, *34*, S101–S108. [[CrossRef](#)]
39. Patankar, S.V. *Numerical Heat Transfer and Fluid Flow*; McGraw Hill: New York, NY, USA, 1980.
40. Versteeg, H.K.; Malalasekera, W. *An Introduction to Computational Fluid Dynamics, the Finite Volume Method*; Pearson: London, UK, 2007.
41. FLUENT Inc. *Documentation Manual—FLUENT 14.3*; FLUENT Inc.: New York, NY, USA, 2013.

42. Hirt, C.W.; Nichols, B.D. Volume of fluid (VOF) method for the dynamics of free boundaries. *J. Comput. Phys.* **1981**, *39*, 201–225. [[CrossRef](#)]
43. Schlichting, H. *Boundary Layer Theory*, 7th ed.; McGraw-Hill: New York, NY, USA, 1979.
44. Morren, G.; Bottiglieri, M.; Bossuyt, S.; Sol, H.; Lecompte, D.; Verleye, B.; Lomov, S.V. A reference specimen for permeability measurements of fibrous reinforcements for RTM. *Compos. Part A Appl. Sci. Manuf.* **2009**, *40*, 244–250. [[CrossRef](#)]
45. Rudd, C.D. *Liquid Moulding Technologies, Resin Transfer Moulding, Structural Reaction Injection Moulding and Related Processing Techniques*; Woodhead Publ: Cambridge, UK, 1997.
46. Srinivasan, V.; Salazar, A.J.; Saito, K. Modeling the disintegration of modulated liquid jets using volume-of-fluid (VOF) methodology. *Appl. Math. Model.* **2011**, *35*, 3710–3730. [[CrossRef](#)]
47. Dos Santos, E.D.; Isoldi, L.A.; Gomes, M.N.; Rocha, L.A.O. *The Constructal Design Applied to Renewable Energy Systems*; Rincón-Mejía, E., de las Heras, A., Eds.; CRC PRESS: Boca Raton, FL, USA, 2017.
48. Gonzales, G.V.; Estrada, E.S.D.; Emmendorfer, L.R.; Isoldi, L.A.; Xie, G.; Rocha, L.A.O.; Dos Santos, E.D. A comparison of simulated annealing schedules for constructal design of complex cavities intruded into conductive walls with internal heat generation. *Energy* **2015**, *93*, 372–382. [[CrossRef](#)]
49. Radiša, R.; Dučić, N.; Manasijević, S.; Marković, N.; Čojbašić, Ž. Casting improvement based on metaheuristic optimization and numerical simulation. *Facta Univ.-Ser. Mech. Eng.* **2017**, *15*, 397–411. [[CrossRef](#)]
50. Hu, J.; Liu, Y.; Shao, X. Study on void formation in multi-layer woven fabrics. *Compos. Part A Appl. Sci. Manuf.* **2004**, *35*, 595–603. [[CrossRef](#)]
51. Schmidt, T.M.; Goss, T.M.; Amico, S.C.; Lekakou, C. Permeability of hybrid reinforcements and mechanical properties of their composites molded by resin transfer molding. *J. Reinf. Plast. Compos.* **2009**, *28*, 2839–2850. [[CrossRef](#)]



© 2020 by the authors. Licensee MDPI, Basel, Switzerland. This article is an open access article distributed under the terms and conditions of the Creative Commons Attribution (CC BY) license (<http://creativecommons.org/licenses/by/4.0/>).